uS

FACULTY OF SCIENCE AND TECHNOLOGY

MASTER THESIS

Study programme / specialisation: **Engineering Structures and Material Science / Specialization in Renewable Energy**	The spring semester, 2022 Open / ~~Confidential~~
Author: **Anastasia Shintami Putri**	……………………………………… (signature author)

Course coordinator: **Knut Erik Teigen Giljarhus** Supervisor(s): **Knut Erik Teigen Giljarhus**

Thesis title: **Simulation of S-Shaped Airfoil for a Bidirectional Tidal Stream Turbine**

Credits (ECTS): 30 ECTS

Keywords: Tidal Turbine Aerodynamic Efficiency Lift to Drag Ratio Lift Coefficient and Drag Coefficient Angle of Attack Computational Fluid Dynamics (CFD) OpenFoam	Pages: 30 + appendix: …………… **Stavanger**, 15th June 2022 date/year

Abstract

The energy supplies in the world mostly rely on fossil fuels which are responsible for increasing the greenhouse effect and global warming by releasing carbon emissions. As global warming is a serious issue for both environment and human health and wellbeing, there is an urgent need to use renewable energy to prevent the environmental problem caused by fossil fuels.

This thesis will discuss the application of tidal stream energy as alternative renewable energy to support sustainable development in society. Tidal energy is more predictable and has higher efficiency than other renewable energy resources like wind energy and wave energy.

This project will analyze and discuss the main component in the airfoil for the horizontal axis tidal turbine. The aerodynamic performance depends on the airfoil design and the sea water flow on the airfoil surface. The results consist of the lift coefficient, the drag coefficient, the aerodynamic efficiency, the performance curve and the off-design performance, the flow pattern, and the pressure.

The airfoil performance will be simulated by the Computational Fluid Dynamics (CFD) to reduce the time and cost experiment. The investigated airfoil designs are NACA – 0012 airfoils and S-Shaped airfoils. Then, the results will be compared to the previous works, to decide the highest performance of the design of the airfoils for the horizontal axis tidal turbine.

Acknowledgments

This thesis is written at the Faculty of Science and Technology, The University of Stavanger in fulfillment of a Master of Science degree in Mechanical and Structural Engineering and Material Science program. I would like to express my gratitude to those who have supported me during this thesis project.

1. To my Almighty God who allows me to pursue my master's degree at the University of Stavanger.
2. To my thesis supervisor, Professor Knut Erik Teigen Giljarhus for his guidance, advice, academic support, and motivation during this project.
3. To my parents and brother who have provided me with the best education and fully supported me despite the long distance we have.
4. To all of my friends in the study program who have helped me during the period of my master's study.

Stavanger, June 2022

Anastasia Shintami Putri

Table of Contents

Abbreviations

NACA   National Advisory Committee for Aeronautics

CFD   Computational Fluid Dynamics

RANS   Reynolds Averaged Navier Stokes

List of Tables

List of Figures

Chapter 1: Introduction

Energy is one of the most essential things to support modern society. Currently, 80% of the energy supplies in the world mostly rely on fossil fuels which are 45% dominated by oil, 36% natural gas, and 19% coal *(Environmental and Energy Study Institute, 2021)*. However, burning fossil fuels is also responsible for increasing the greenhouse effect and global warming by releasing carbon emissions. The global average temperature has reached 1.1° C in the last 10 years and it was recorded as the warmest decade (*European Commission, u.d.*). Global warming is a serious issue that can affect both environment and human health and wellbeing. However, the accessible supply of energy resources is required to meet the market demand. This condition creates its challenge to maintain the increasing temperature to below 2° C by reducing the dependency on fossil energy consumption and converting it into renewable energy.

Renewable energy technologies are one of the solutions to prevent global warming as well as the environmental problem caused by the large consumption of fossil fuels. The energy sources that come from the Sun, wind, waterfall, and ocean cannot be depleted and are produced in long term. Furthermore, they have less environmental impact which means they support sustainable development in society. The technologies are divided into old technologies (hydropower, geothermal, and biomass) and new technologies (solar, wind, and ocean energy).

In 2020, The utilization of renewable energy technologies in the world made up 29% of electricity generation, and 16.8% of it comes from hydropower (*Center for Climate and Energy Solutions, u.d.*). The number of global renewable power capacity production was added to over 256 GW, led by wind power and solar photovoltaic (PV) which contributed 10% increase in total installed renewable power capacity (*REN21, 2021*). In Norway, 98% of the electricity production comes from renewable energy which makes Norway the highest electricity producer of renewable resources in Europe. The total electricity production is generated 90% from hydropower, 6.4% from wind power, and 2% from thermal power plants (*Energi Fakta Norge, 2021*). Meanwhile in Indonesia, 82% of the power generation mostly still relies on fossil fuels and only a little amount of power generation comes from renewable energy which produces 8% from hydroelectric, 6% from geothermal energy, and 4% from other resources like biomass *(U.S. Energy Information*

Administration, 2021). In the future, renewable power capacity production is predicted to increase 23% by 2025 and 31% by 2050 (*Statista, 2021*).

The earth's surface consists of 71% water and 29% land which makes the availability of ocean energy large and promising to generate electricity. If all of the electric power is generated by ocean energy technology, it can supply 10% of the world's energy consumption. The advantages of ocean energy are more predictable and very high in efficiency which is 80% compared to other renewable energy resources and the density of the seawater is higher than the density of air, so the power produced by ocean energy is larger than the wind energy in the same size of turbine. However, the investment in the installation and maintenance of ocean energy technology is still more expensive than other types of renewable energy.

There are three ways to extract ocean energy which are tidal current energy, wave energy, and ocean thermal energy. The tidal current energy converts the potential energy and kinetic energy of different sea levels that are caused by tidal effects to move the seawater, then push the turbine and generate the electricity. The tides are affected by the gravitational attraction and the rotation of the Earth, the Sun, and the Moon. Meanwhile, the wave energy is affected by the wind blowing over the ocean surface. Then, the ocean thermal energy conversion (OTEC) uses the principle of a thermodynamic cycle which depends on the water temperature gradient in the ocean and the surface. The temperature gradient should be higher or equal to 20° C which is only possible in tropical and equator areas. Amongst the ocean energy, the tidal current energy and the wave energy devices have the highest efficiency but the ocean thermal energy conversion systems have larger energy resources. Tidal current energy density is also higher than the other type of ocean energy density. It is also more predictable than wave energy since the ocean experiences high tides and low tides twice a day.

Tidal energy can be created by several technologies which are tidal barrages and tidal stream turbines. The principle of a tidal barrage system is similar to a hydropower turbine which harnesses the potential energy from different sea levels of tides (low and high tides) by using the dam that is known as a barrage across the bay or estuary. The sluice gates on the barrage allow the tidal basin to fill on the incoming high tides (flood tides) and exit through the turbine system on the outgoing tides (ebb tides) (*Sheth & Shahidehpour, 2005*). The minimum tidal range to economically generate the electricity is required at least 7 meters. The largest tidal barrage power plants have

been installed in the Sihwa Lake Tidal Power Station in South Korea. It produces 254 MW of electricity and the oldest tidal barrage power plants have been operating in La Rance, France with a 240 MW electricity generation capacity (*U.S. Energy Information Administration, 2021*).

The other technology of tidal energy is a tidal stream turbine. The principle of a tidal stream turbine generator is similar to a wind turbine, but it is installed underwater and uses the kinetic energy of underwater movement to generate electricity. There are two types of tidal stream turbine generators, the horizontal axis tidal turbine (HATT) and the vertical axis tidal turbine (VATT). The turbine blades in the horizontal axis tidal turbine rotate in the same direction as the seawater movement, while the turbine blades in the vertical axis tidal turbine rotate perpendicular to the seawater movement. This type of tidal energy generator is less environmental impact on marine life than the tidal barrage, which can prevent during the installation.

In Norway, tidal energy is considered the third ocean energy resource after offshore wind and wave energy. The tidal ranges are modest. In Oslo, the maximum tidal range is 72 cm but the maximum observed sea-level range is 308 cm. Then, in Bodø south of Lofoten, the maximum tidal range is 333 cm with a mean spring tidal range of 236 cm (*Grabbe, 2009*). Meanwhile, the tidal ranges in Indonesia are relatively high. In the Larantuka Strait, which located between East Flores and Adunara Island, is the water depths are up to 20 – 25 meters and link the Flores Sea in the North to the Flores Strait in the south. The tidal ranges in the Flores Sea are slightly larger than 1 meter to 1.5 meters in Flores Strait. The peak velocity of currents at spring tide in the Larantuka strait is 3 to 4 m/s and the power density at some locations can exceed 6 kW/m^2 (*Orhan, 2015*).

The aerodynamic characteristics of airfoils as well as the mechanical design and fabrication of the tidal stream turbine blade are important for the blade performance. The aerodynamic designs need to consider the pressure distribution on the airfoil's surface, the minimum coefficient of pressure (C_P), coefficient of lift (C_L), coefficient of drag (C_D), and lift-to-drag ratio (L/D). The airfoil design also requires delayed stall and free cavitation while maintaining a higher lift coefficient and lift-to-drag ratio (*Goundar, 2013*). Moreover, mechanical design and fabrication play an important role in the blade as it is relevant to the blade strength and stiffness. The structure design should be based on the hydrodynamic design results and the load distribution on the blade surface under working conditions (*Li, 2016*).

The objective of this thesis will be focused on the horizontal axis tidal turbine aerodynamic performance which depends on the airfoil design and the sea water flow on the airfoil surface. The baseline airfoil design is NACA-0012 airfoils. Then, as a comparison, it will be analyzed the performance of S-Shaped airfoil.

This thesis consists of five chapters. Chapter 1 is an introduction that explains the background of choosing the topic. Chapter 2 is a fundamental theory and methodology of the tidal turbine. Chapter 3 is a computational setup as the setup for the geometry for the airfoils and the simulation. Chapter 4 is the results and discussion. And chapter 5 is the conclusion of this project.

Chapter 2: Fundamental Theory and Methodology

2.1. Numerical Analysis

The principle of a tidal streams turbine generator is similar to a wind turbine, thus the airfoil design analysis for a horizontal axis tidal turbine can use the same approach as an airfoil for a horizontal axis wind turbine. However, there are major differences in the engineering for tidal streams turbine because of the higher water density compared with air and the slower rotation speed.

This part will be explained two main requirements for designing airfoils for horizontal axis tidal turbines and the essential components for analyzing the blade elements.

2.1.1. Airfoil Requirements for Tidal Turbine

The airfoil for tidal turbine design needs to consider two main requirements such as the structural design and the aerodynamic design requirements.

A.   Structural Design Requirements

In the structural design requirements, the maximum airfoil thickness must be able to accommodate the structure necessary to ensure the blade strength and stiffness (*Grasso, 2012*). Thick airfoil sections generally have a lower lift-to-drag ratio, therefore special consideration is made for increasing the lift of thick airfoil sections (S*chubel & Crossley, 2012*). The location of the maximum thickness along the chord is also important. When an airfoil is designed, the other airfoils along the blade should be considered to guarantee constructive compatibility. Therefore, the structural design should be based on the aerodynamic design results and the load distribution on the blade surface under working conditions (*Li, 2016*).

B.   Aerodynamic Design Requirements

The aerodynamic designs need to consider the pressure distribution on the airfoil's surface, the minimum coefficient of pressure (C_P), coefficient of lift (C_L), coefficient of drag (C_D), and the lift-to-drag ratio (L/D). The non-uniform current speed and direction, the shear profile in the tidal flow, and the influence of the water depth and the free surface make the aerodynamic designs complicated and challenging. Therefore, the designs require delayed stall and free cavitation while maintaining a higher lift coefficient, lower drag ratio, and higher lift-to-drag ratio over a various range angles of attack (*Goundar, 2013*).

The most important parameter for the blade design is the aerodynamic efficiency which can be defined as:

$$\text{Aerodynamic Efficiency} = \frac{\text{Coefficient of Lift}}{\text{Coefficient of Drag}} = \frac{C_L}{C_D} \qquad (2.1)$$

To obtain good turbine performance, the aerodynamic efficiency should be as high as possible which is usually greater than 30 for blade design.

2.1.2. Main Component for Analyzing the Airfoil Elements

The initial tidal turbine design requires the blade element momentum (BEM) theory which consists of four main aerodynamic force components. Those components are lift force, drag force, axial force, and tangential force. It is illustrated in the diagram of aerodynamic force analysis of blade elements in **Fig. 2.1.**
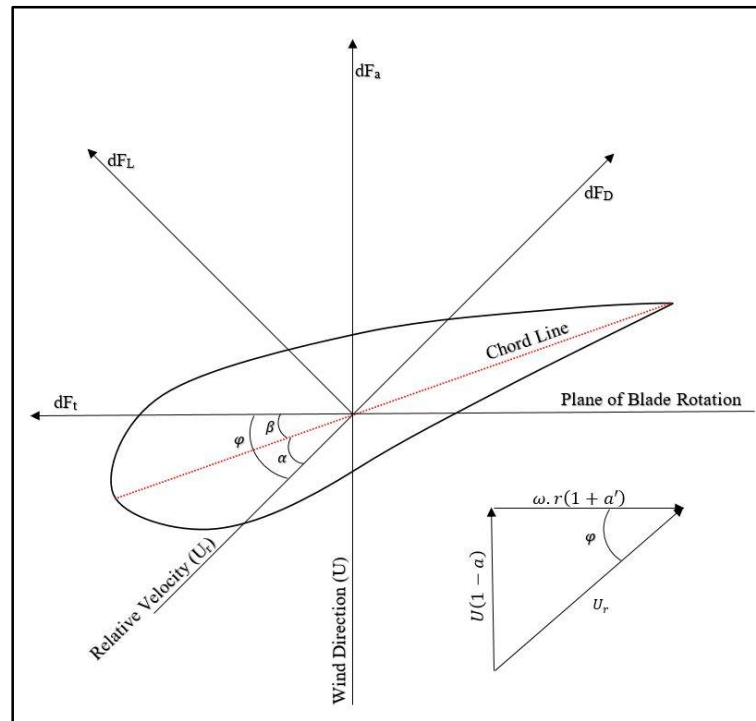

Figure 2.1 The Diagram of Aerodynamic Force Analysis of Blade Elements

A. Lift Force

The tidal turbine blades work due to the lift force. The lift force is perpendicular to the relative velocity of the water flow. The water flows in the upper of the airfoil travel longer than on the lower surface and the velocity over the top is higher than on the bottom. The lower pressure over

the top makes the blade lift. The lift force on the blade elements can be obtained as the following formula:

$$dF_L = \frac{1}{2} . \rho . U_r{}^2 . C_L . c . dr \qquad (2.2)$$

Where F_L is the lift force, ρ is the density of seawater, U_r is the relative water velocity, C_L is the lift coefficient, and c is the chord length.

B.   Drag Force

The tidal turbine blades have a drag force that is parallel to the relative velocity of the water flow and increases with the angle of attack. The drag force decreases the force that is given by the lift force. The drag force on the blade elements can take into account by the following formula:

$$dF_D = \frac{1}{2} . \rho . U_r{}^2 . C_D . c . dr \qquad (2.3)$$

Where F_D is the drag force, ρ is the density of seawater, U_r is the relative water velocity, C_D is the drag coefficient, and c is the chord length.

C.   Axial Force

The axial velocity direction in the tidal turbine blade has the same direction as the incoming water flow. The axial force is defined as the resultant of the lift force and the drag force that can take into account by the following formula:

$$dF_a = dF_L . \text{Cos}\varphi + dF_D . \text{Sin}\varphi = \frac{1}{2} . \rho . U_r{}^2 . C_n . c . dr \qquad (2.4)$$

Where C_n is the axial coefficient.

$$C_n = C_L . \text{Cos}\varphi + C_D . \text{Sin}\varphi \qquad (2.5)$$

D.   Tangential Force

The tangential velocity direction in the tidal turbine blade work in the opposite direction to the blade rotation. The tangential force of the blade element can be obtained as the following formula:

$$dF_t = dF_L . \text{Sin}\varphi - dF_D . \text{Cos}\varphi = \frac{1}{2} . \rho . U_r{}^2 . C_t . c . dr \qquad (2.6)$$

Where C_t is the tangential coefficient.

$$C_t = C_L . \text{Sin}\varphi - C_D . \text{Cos}\varphi \qquad (2.7)$$

E.   Relative Velocity of Water Flow and Angle of the Relative Velocity (φ)

The relative velocity of water flow and the angle of the relative velocity can be known by the trigonometric relationship in Fig. 2.1. The relative velocity of water flow can be obtained as:

$$U_r = \sqrt{[U(1-a)]^2 + [\omega.r(1+a')]^2} \qquad (2.8)$$

The angle of the relative velocity (φ) is defined as the angle between the plane of blade rotation and the relative velocity. It can be obtained as:

$$\varphi = tan^{-1}\left[\frac{U(1-a)}{\omega.r(1+a')}\right] \qquad (2.9)$$

F.   Angle of Attack (α) and Pitch Angle (β) of the Blade Element

The angle of attack (α) is defined as the angle between the chord line and the relative velocity which is an important parameter to optimize the lift. The lift coefficient increases as the higher angle of attack until it reaches the critical angle. At the critical angle of attack, the lift coefficient will decrease and the drag coefficient will increase dramatically. This condition makes the blade in a *stall* position. To prevent the *stall*, the angle of attack has to be maintained at slightly less than the maximum angle of attack, when the blade is in the maximum lift and drag ratio.

The pitch angle (β) is defined as the angle between the chord line and the plane of blade rotation that can be used to control the blade rotation. The correlation between the angle of the relative velocity, the angle of attack, and the pitch angle can be written as:

$$\alpha = \varphi - \beta \qquad (2.10)$$

2.2.   Computational Fluid Dynamics (CFD)

The turbulence flow in the airfoil performance is commonly analyzed by the Computational Fluid Dynamics (CFD) to reduce the time and cost experiment. The calculation will use the Reynolds Averaged Navier Stokes (RANS) equation to develop the turbulence model in the airfoil simulation. The turbulence model used is the Spalart – Allmaras (S.A) model that solves an equation for turbulent eddy viscosity (υ̃). The semi–implicit method for pressure linked equation (SIMPLE) is an effective algorithm for solving the pressure velocity coupling problem under the steady-state condition.

The airfoil performance analysis will use the Open Source Field Operation and Manipulation (OpenFoam) software to simulate different types of airfoil shape cases.

2.2.1. Construct2D

In the OpenFoam software, the grid generation uses Construct2D to create 2D grids for CFD computations on airfoils. The grids are generated in plot3D format which requires the airfoil geometry. Construct2D can create grids with O topology for airfoils with a blunt trailing edge or C topology for airfoils with a sharp trailing edge (*Sourceforge, 2018*).

The grid sensitivity parameters to generate the grid mesh are defined as the Number of Points on Surface (NSRF), the Leading Edge Point Spacing (LESP), the Trailing Edge Point Spacing (TESP), the chord length, and radius. The grid sensitivity parameters are illustrated in **Fig. 2.2.**
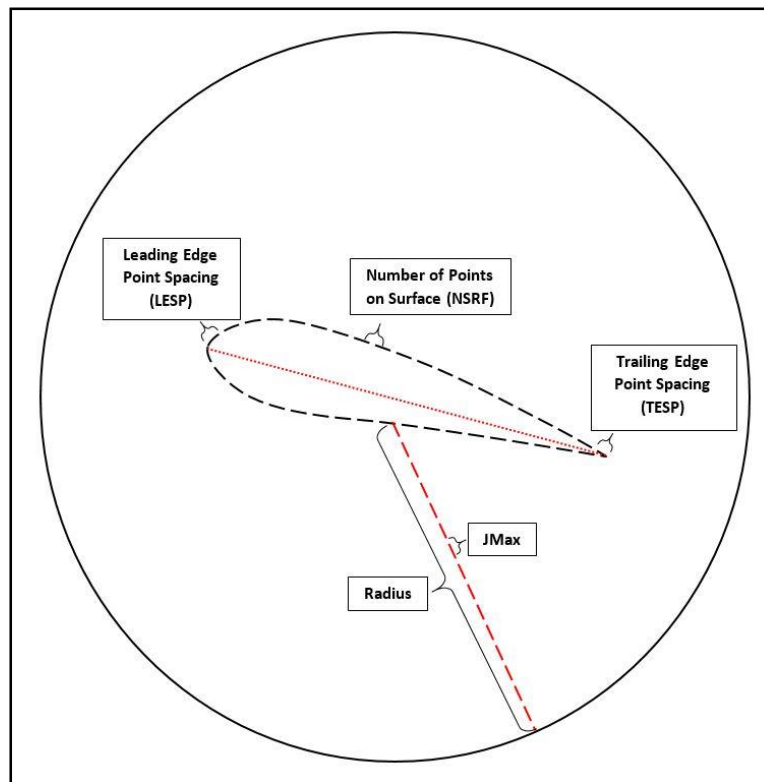

Figure 2.2 The Grid Sensitivity Parameters in Construct2D

Chapter 3: Computational Setup

The airfoil shape cases that will be analyzed are NACA – 0012 airfoils and S–Shaped Airfoil.

3.1. Baseline of NACA – 0012 Airfoil

The airfoil performance analysis will be simulated on two-dimensional NACA – 0012 airfoils. The four digits' number in the airfoils represent the airfoil geometry properties. 00 shows that the airfoil is symmetrical and does not have a chamber, then 12 shows that the maximum thickness is 12% of the chord length ratio. The geometry of NACA – 0012 airfoils is illustrated in **Fig. 3.1.**
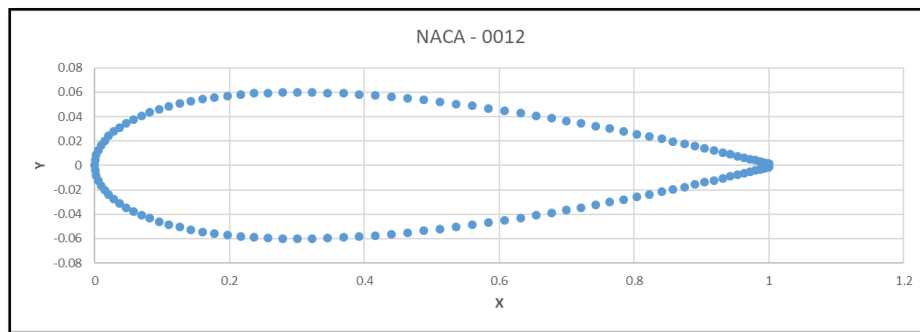

Figure 3.1 The Geometry of NACA – 0012 Airfoils

To validate the geometry and to determine the minimum grid resolution, primarily the mesh will be tested into different grids sensitivity tests (very coarse, coarse, medium, and fine grids) in the various angle of attack from -5° to 20°. The Reynold number for this simulation is 6 x 10^6. Some parameters need to be adjusted to start generating the grid mesh. **Table 3.1.** shows the grid sensitivity parameter adjustment for different grid systems.

Table 3.1 The Grid Sensitivity Parameter Adjustment for Different Grid Systems

Grid	Surface Points NSRF	Leading Edge Spacing Point LESP	Trailing Edge Spacing Points TESP	Volume Point Jmax
Very Coarse	125	4.0E-03	5.2E-04	50
Coarse	188	3.0E-03	3.9E-04	75
Medium	250	2.0E-03	2.6E-04	100
Fine	375	1.5E-03	1.95E-04	150

Firstly, all of the adjusted grid mesh parameters in different grids need to be generated at the angle of attack of 0° by setting the velocity to 60 m/s. The generating grid result can be viewed in the *paraview* to make sure that the geometry is correct. After the grid is generated, continue the

simulation by using *simpleFoam* command for some iterations. Then, plot the lift and drag coefficient to confirm that the coefficient is already stable in certain iterations. In this case, the simulation stops in the 5000 iterations that can be adjusted in the *controlDict* file. Since the validation gives a similar number of lift and drag coefficient results in different grids, it is decided to choose the medium grid for other angles of attack simulations.

Repeating above steps into the various angle of attack simulation in the medium grid. After all the simulations have been done, plot the lift and drag coefficient results into different angles of attack chart. Based on the angle of attack chart, it can be recognized the optimum angle of attack before the *stall* position and the maximum lift and drag ratio. Compare the simulation result with the experimental data.

3.2.   S–Shaped Airfoil

The second airfoil case will be simulated on S–Shaped airfoils. This case is taken based on the experiment on the cascade of S–Shaped hydrofoil on a fully reversible pump turbine *(T & Chatterjee, 2015)*. The geometry of S–Shaped airfoil is illustrated in the **Fig. 3.2.**
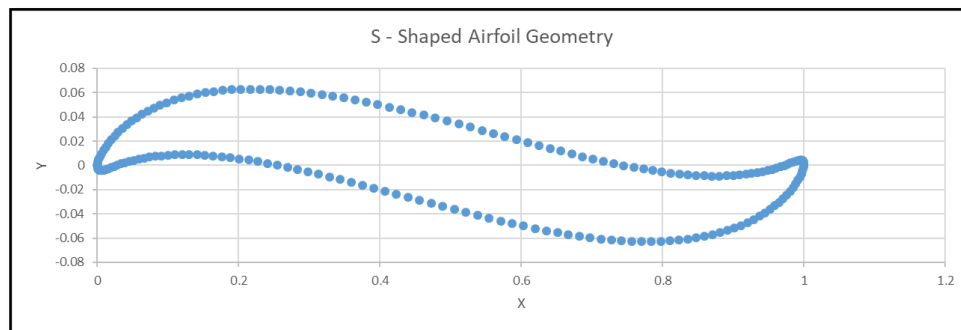

Figure 3.2 The Geometry of S–Shaped Airfoil

The grid mesh of S–Shaped airfoil is generated at the velocity of 20 m/s by setting up the grid sensitivity parameters. Those parameters consist of the number of points on surface (NSRF) and the volume point (Jmax) which value 250 and 100 respectively. The Reynold number for this case is 2×10^6. Since the geometry of the airfoil is sharp on each edge, the leading edge has the same value as the trailing edge which is 0.5×10^{-3}. After the grid is generated, simulated various angles of attack from 0° to 20° in some iterations. In this case, the simulation stops in the 2000 iterations. Then, post-processing the result by plotting the lift and drag coefficient into different angles of attack chart.

Chapter 4: Results and Discussion

4.1.   Baseline of NACA – 0012 Airfoils

In the NACA – 0012 airfoils case, the medium grid sensitivity has been chosen. At higher angles of attack, some of the simulations diverge from the default numerical setup. For these cases, convergence was achieved by first simulating with the first-order *upwind* scheme for 200 iterations to stabilize it, before switching to the *linearUpwind* scheme for the remainder of the simulation. The post-processing results are analyzed by plotting the lift coefficient, the drag coefficient, and the lift-to-drag ratio into various angles of attack from -5° to 20°, then comparing the result with the experimental data. The simulation results in various angles of attack for lift coefficient, drag coefficient, and lift-to-drag ratio are summarized in **Table 4.1.**

Table 4.1 The Simulation Result for NACA – 0012 Airfoils

Angle of Attack (AoA)	Lift Coefficient (Cl)	Drag Coefficient (Cd)	Lift to Drag Ratio
-5	-0.5480605	0.009460491	-57.93150694
0	0.00240126	0.008310426	0.288945476
5	0.5529878	0.009478269	58.3426995
10	1.07386	0.01366795	78.56774425
15	1.504614	0.02389885	62.95759001

4.1.1. Lift Coefficient

The plot of lift coefficient in different angle of attack simulation results compared to the experimental data can be seen in **Fig. 4.1.**
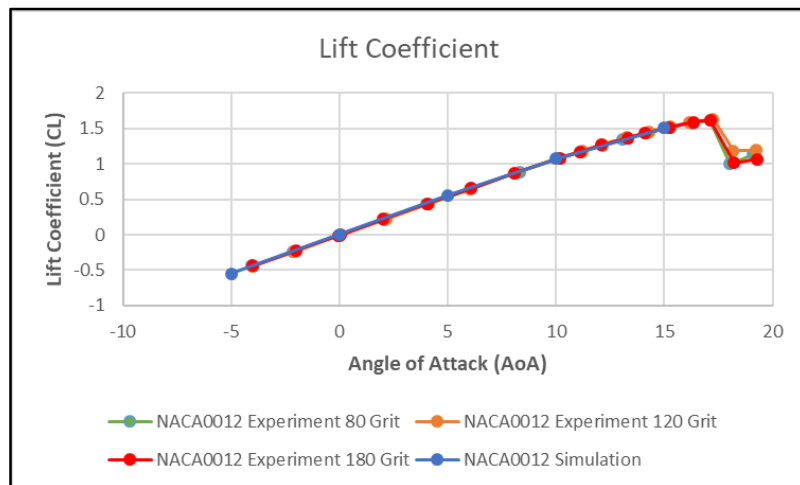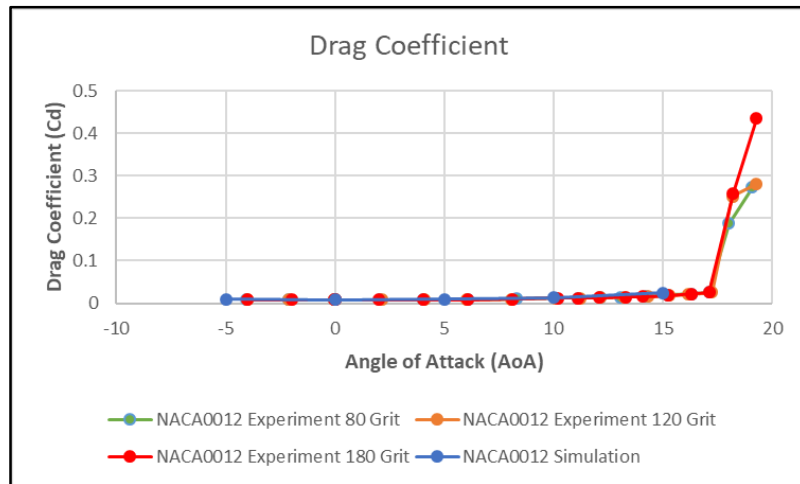

Figure 4.1 The Plot of Lift Coefficient in Various Angles of Attack for NACA – 0012 Airfoils

The chart shows that the lift coefficient increases with the higher angle of attack until it reaches the critical angle. The critical angle of attack is 17.13° and the maximum lift is 1.62 before the airfoil loses its ability to lift and starts to be in *stall* position.

4.1.2. Drag Coefficient

The plot of the drag coefficient at different angles of attack simulation results compared to the experimental data can be seen in **Fig. 4.2.**

Figure 4.2 The Plot of Drag Coefficient in Various Angles of Attack for NACA – 0012 Airfoils

The chart shows that the drag coefficient slightly increases with the higher angle of attack until it reaches the critical angle. At the critical angle of attack, the drag coefficient dramatically increases. The maximum drag coefficient is 0.025.

4.1.3. Aerodynamic Efficiency

The aerodynamic efficiency can be obtained by calculating the lift-to-drag ratio. The plot of the lift-to-drag ratio in various angles of attack for NACA – 0012 airfoils in comparison to the experimental data can be seen in **Fig. 4.3.**
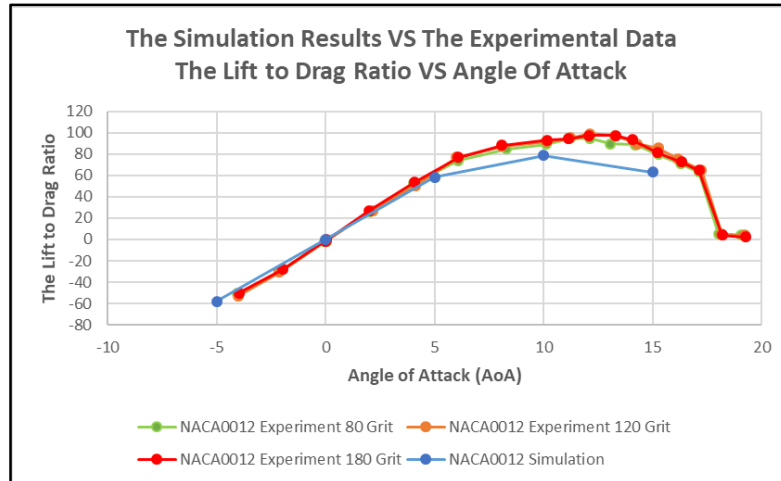
Figure 4.3 The Plot of Lift to Drag Ratio in Various Angles of Attack for NACA – 0012 Airfoils

The chart shows that the lift-to-drag ratio in the simulation is identical to the experimental data at a lower angle of attack. However, in the higher angle of attack which is above 5°, the simulation gives a slightly lower lift-to-drag ratio results.

4.1.4. Performance Curve and Off–Design Performance

The NACA – 0012 airfoils performance is analyzed by choosing the critical angle of attack from the lift coefficient and the lift-to-drag ratio. The chart can be seen in **Fig. 4.4.**
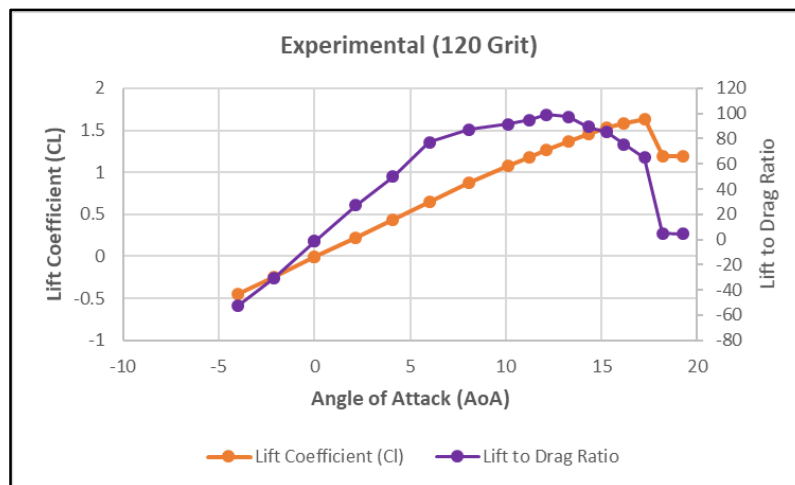

Figure 4.4 Performance Curve and Off-Design Performance for NACA – 0012 Airfoils

The chart shows that the maximum lift coefficient and the aerodynamic efficiency at the angle of attack 17.24° are 1.63 and 64.89 respectively. Then, the lift coefficient and the aerodynamic efficiency design at the angle of attack 12.13° are 1.27 and 99.22. The slope for this airfoil can be obtained by subtracting the aerodynamic efficiency design to the aerodynamic efficiency

maximum, then dividing by the different angles of attack ($\Delta\alpha$). The slope for NACA - 0012 is 6.72. The off–design performance for this airfoil is 5.11 which is quite close to the *stall* point.

4.1.5. Water Flow Pattern

The water flow patterns in various angles of attack can analyze the water flow direction at different angles. It can be shown in **Fig. 4.5.**
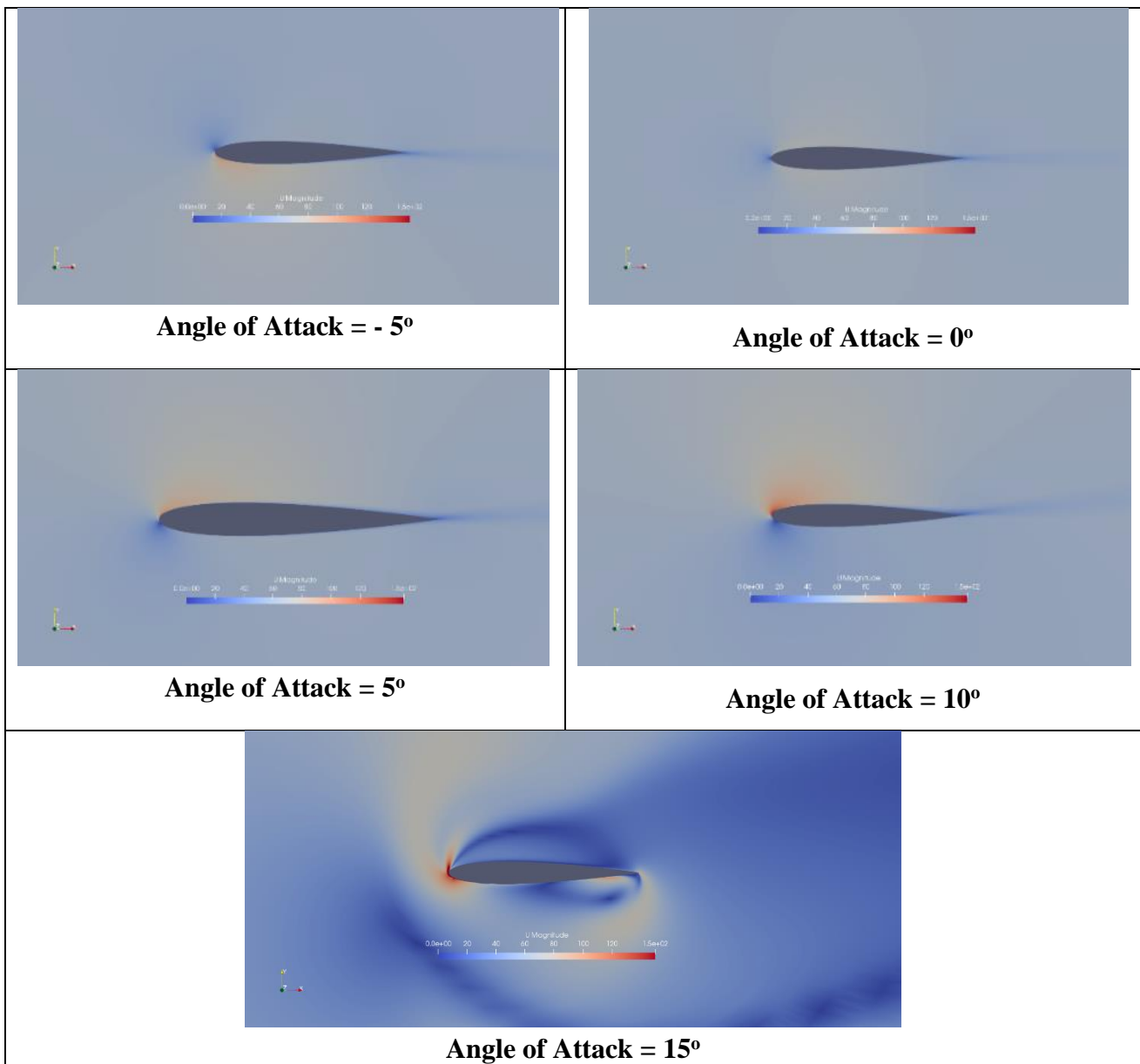

Angle of Attack = - 5º

Angle of Attack = 0º

Angle of Attack = 5º

Angle of Attack = 10º

Angle of Attack = 15º

Figure 4.5 The Water Flow Pattern in various angles of attack for NACA - 0012 Airfoils

The pictures show that the water flows separately through the leading edge to the upper and lower surface of the airfoils to the trailing edge. In the angle of attack of -5º, the velocity of the water flow is lower on the upper surface and higher on the lower surface. However, in the higher

angle of attack, the water flow is higher on the upper surface and lower at the bottom. The larger water flow separation on the trailing edge can increase the ability for airfoils to lift until it reaches the critical angle. At the angle of attack of 15º, the velocity of the water flow spreads unevenly around the airfoil which means the airfoil starts to lose its ability to lift and close to the *Stall* position.

4.1.6. Pressure

The pressure patterns in the various angles of attack can analyze the airfoil's ability to lift at different angles of attack. It can be shown in **Fig. 4.6**.
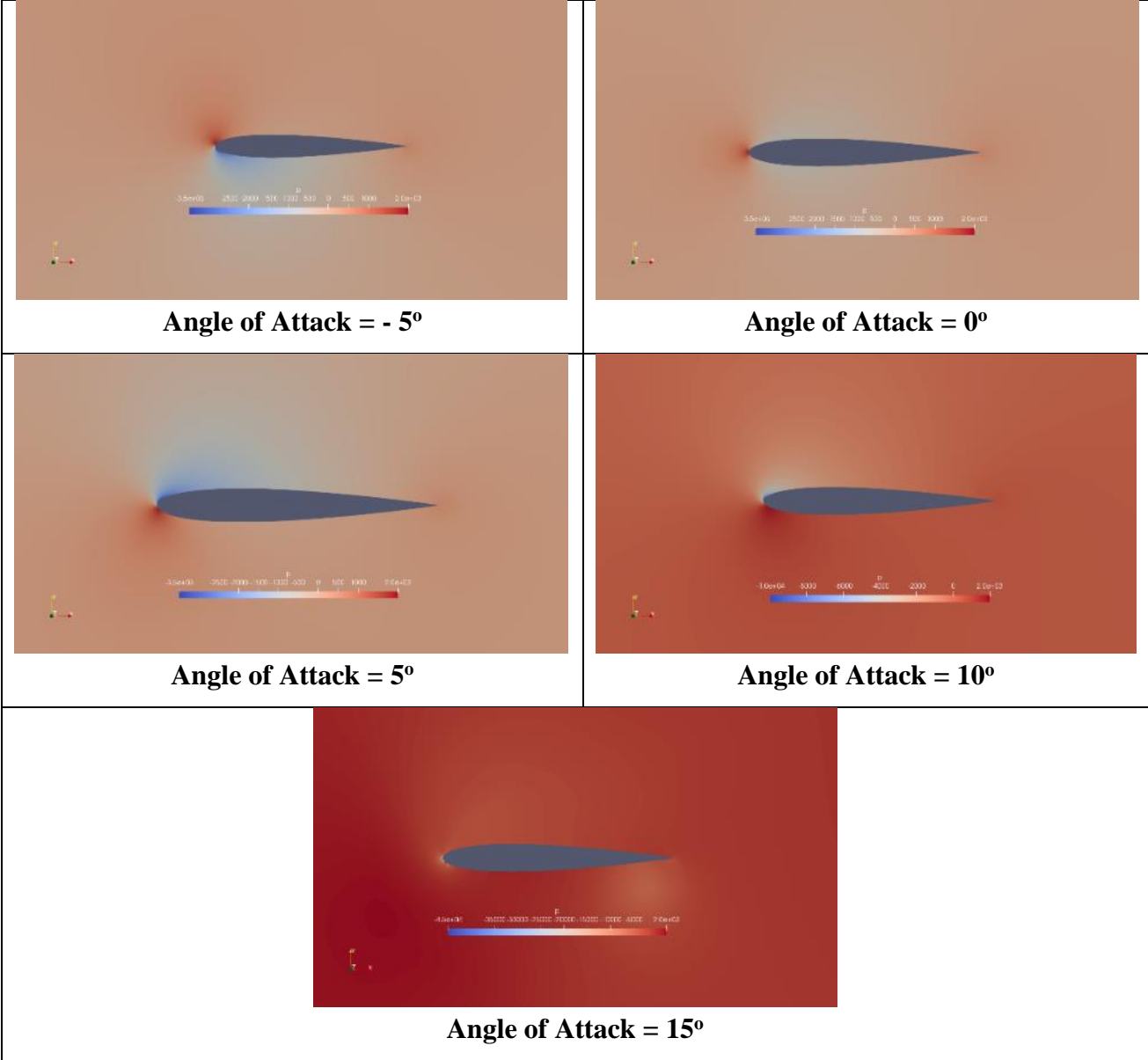

Angle of Attack = - 5º	**Angle of Attack = 0º**
Angle of Attack = 5º	**Angle of Attack = 10º**
Angle of Attack = 15º	

Figure 4.6 The Pressure in Various Angles of Attack for NACA – 0012 Airfoils

The pictures show that the pressure is higher on the upper surface of the airfoils in the lower angle of attack. It means the lift coefficient is still low and the airfoil performance is in the minimum lift. On the other hand, in the higher angle of attack, the pressure over the top surface of the airfoils is lower than on the bottom which drives the airfoils to lift. In the angle of attack of 15°, the pressure around the airfoils is very high and takes the airfoils in the *Stall* position.

4.2. S–Shaped Airfoil

The post-processing results are analyzed by plotting the lift coefficient, the drag coefficient, and the lift-to-drag ratio into various angles of attack from 0° to 20°. The simulation results are summarized in **Table 4.2.**

Table 4.2 The Simulation Result for S–Shaped Airfoils

Angle of Attack (AoA)	Lift Coefficient (Cl)	Drag Coefficient (Cd)	Lift to Drag Ratio
0	-0.2704273	0.03201721	-8.446310594
2	-0.103113	0.02618988	-3.937131442
4	0.07488892	0.02504188	2.990547036
6	0.259577	0.02831468	9.167576678
8	0.4447779	0.03609852	12.32122259
10	0.6209574	0.04859263	12.7788391
12	0.7699949	0.06588796	11.68642799
14	0.8458484	0.08715249	9.705384206
16	0.7896018	0.1129469	6.990911658
18	0.7169312	0.1455191	4.926715462
20	0.67062	0.184398	3.636807341

4.2.1. Lift Coefficient

The plot of lift coefficient in different angle of attack simulation results for S–Shaped Airfoils can be seen in **Fig. 4.7.**
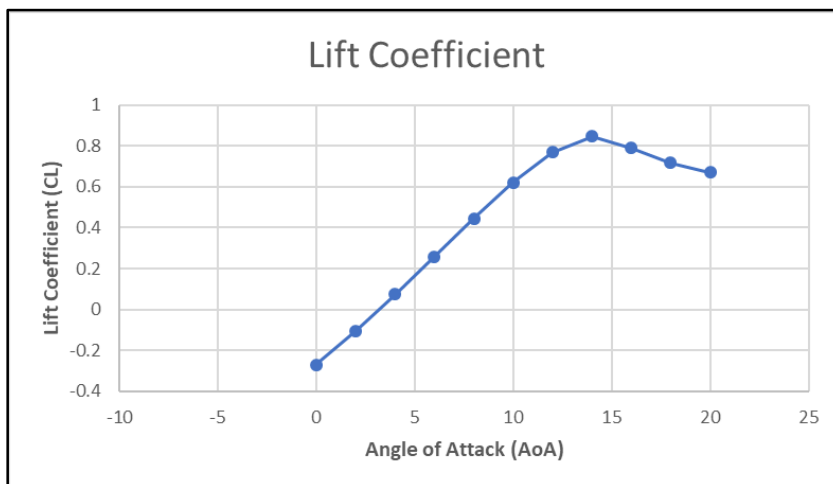

Figure 4.7 The Plot of Lift Coefficient in Different Angles of Attack for S–Shaped Airfoils

The chart shows that the maximum lift coefficient at the critical angle of attack 14° is 0.85 before the airfoil loses its ability to lift and starts to be in the *stall* position.

4.2.2. Drag Coefficient

The plot of the drag coefficient at the different angles of attack simulation result for S – Shaped airfoils can be seen in **Fig. 4.8.**
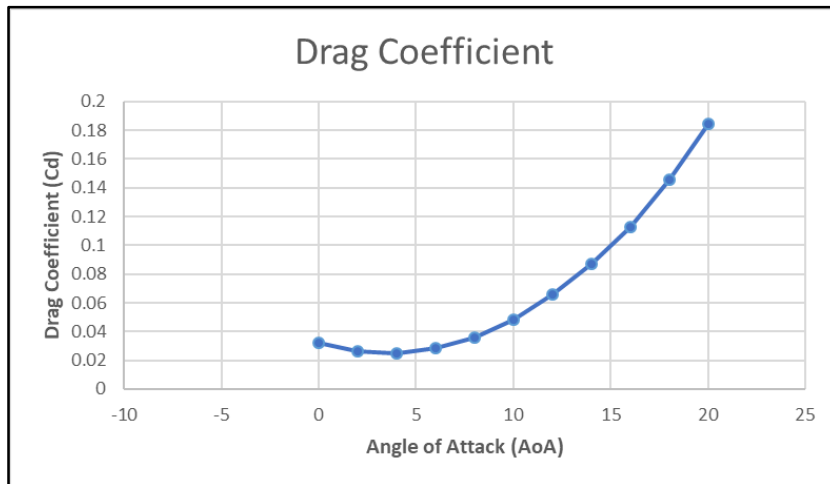

Figure 4.8 The Plot of Drag Coefficient in Different Angles of Attack for S–Shaped Airfoils

The chart shows that the drag coefficient gradually increases with the higher angle of attack. At the critical angle of attack, the drag coefficient is 0.087.

4.2.3. Aerodynamic Efficiency

The plot of the lift-to-drag ratio in various angles of attack for S – Shaped airfoils can be seen in **Fig. 4.9.**
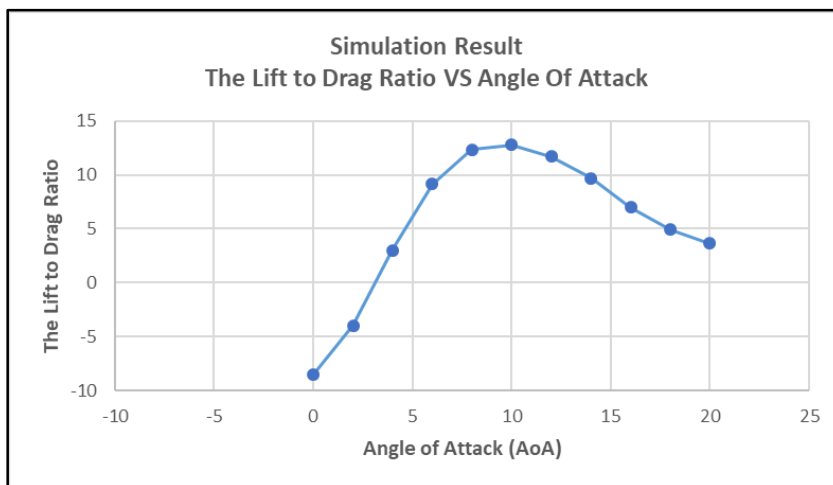
Figure 4.9 The Plot of Lift to Drag Ratio in Various Angles of Attack for S–Shaped Airfoils

The chart shows that the maximum lift-to-drag ratio for S–Shaped airfoils is 12.78 at the angle of attack of 10°.

4.2.4. Performance Curve and Off–Design Performance

The S–Shaped airfoil performance curve and the drop–off design performance can be seen in **Fig. 4.10.**
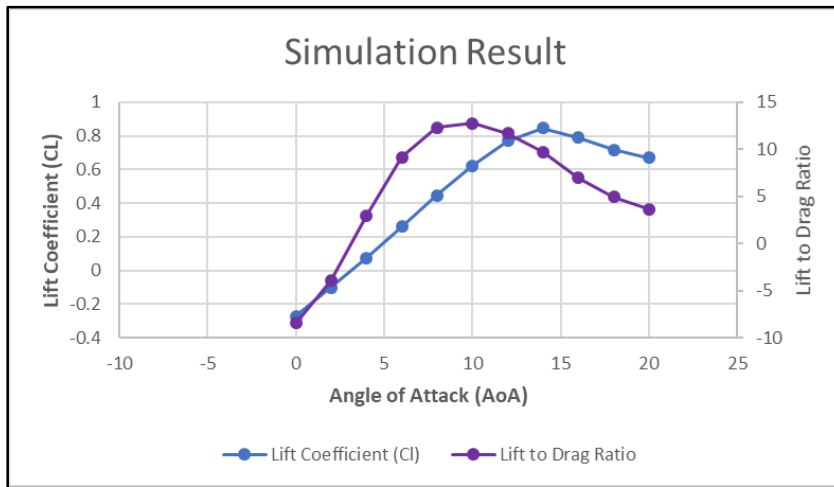

Figure 4.10 The Performance Curve and Off Design Performance for S–Shaped Airfoils
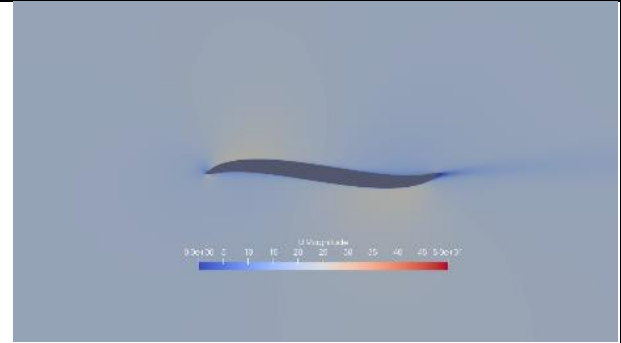
The chart shows that the maximum lift coefficient and the aerodynamic efficiency at the angle of attack 14° are 0.85 and 9.71 respectively. Then, the lift coefficient and the aerodynamic efficiency design at the angle of attack 10° are 0.62 and 12.78. The slope for this airfoil can be obtained by subtracting the aerodynamic efficiency design to the aerodynamic efficiency maximum, then dividing by the different angles of attack ($\Delta\alpha$). The slope for S–Shaped is 0.77. The off–design performance for this airfoil is 4 which is very close to the *stall* point.
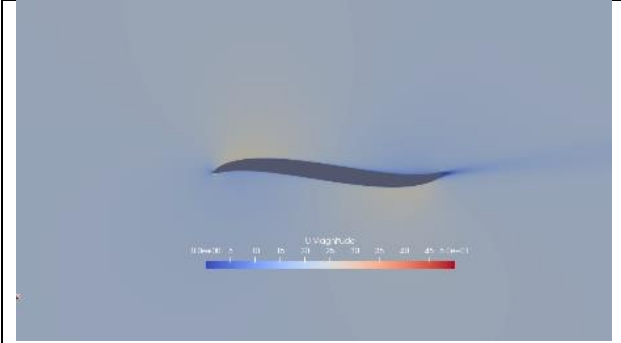
4.2.5. Water Flow Pattern

The water flow pattern in various angles of attack can analyze the water flow direction at different angles. It can be shown in **Fig. 4.11.**
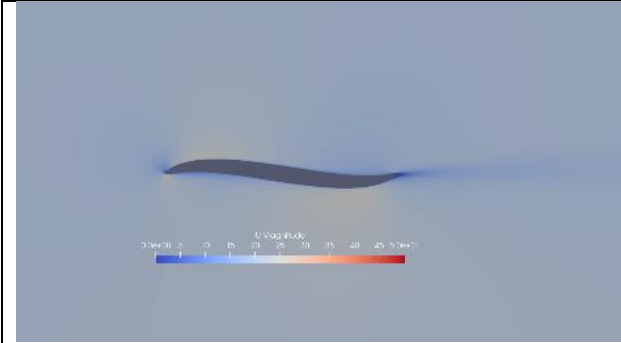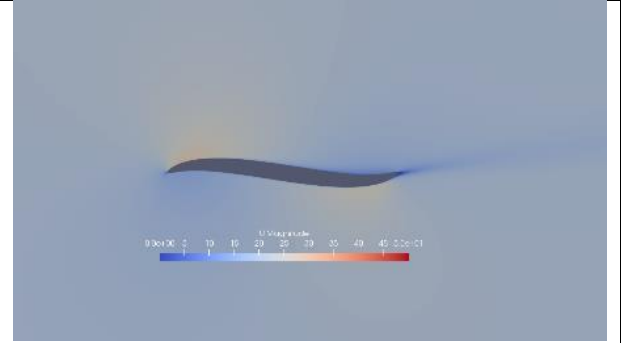
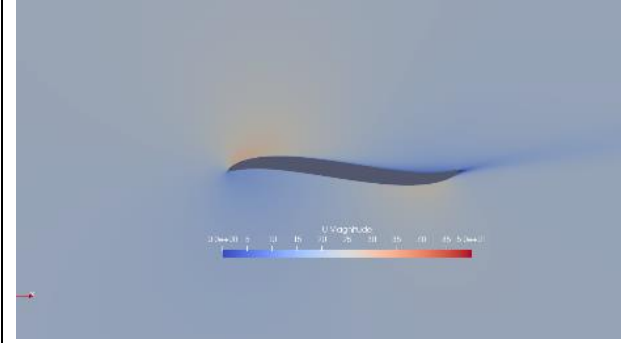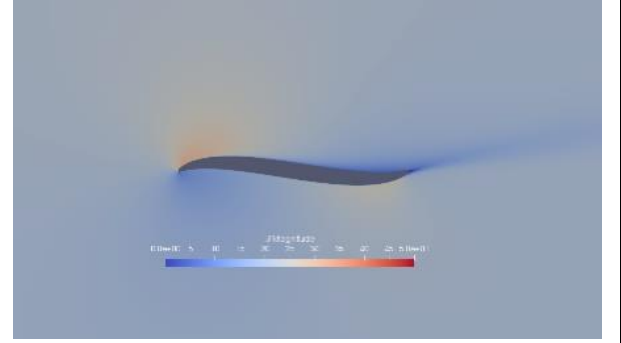|	
Angle of Attack = 0⁰	**Angle of Attack = 2⁰**
Angle of Attack = 4⁰	**Angle of Attack = 6⁰**
Angle of Attack = 8⁰	**Angle of Attack = 10⁰**
Angle of Attack = 12⁰	**Angle of Attack = 14⁰**

Angle of Attack = 16º	**Angle of Attack = 18º**
Angle of Attack = 20º	
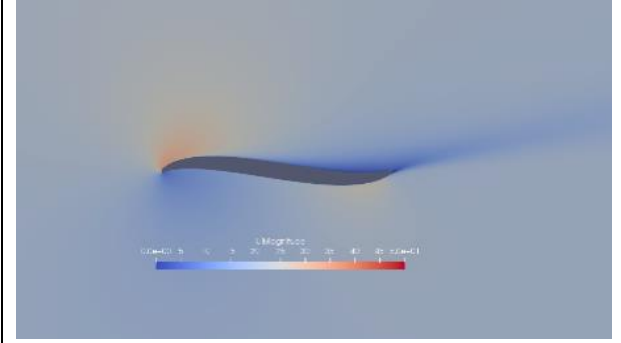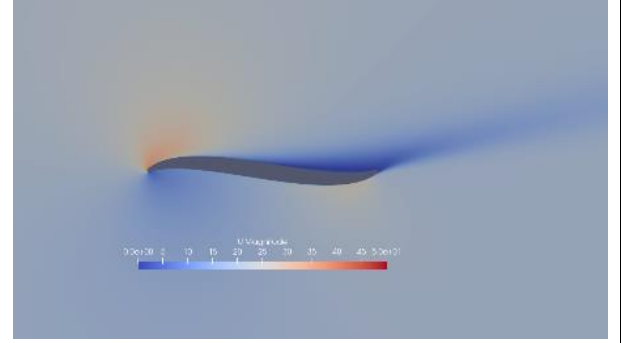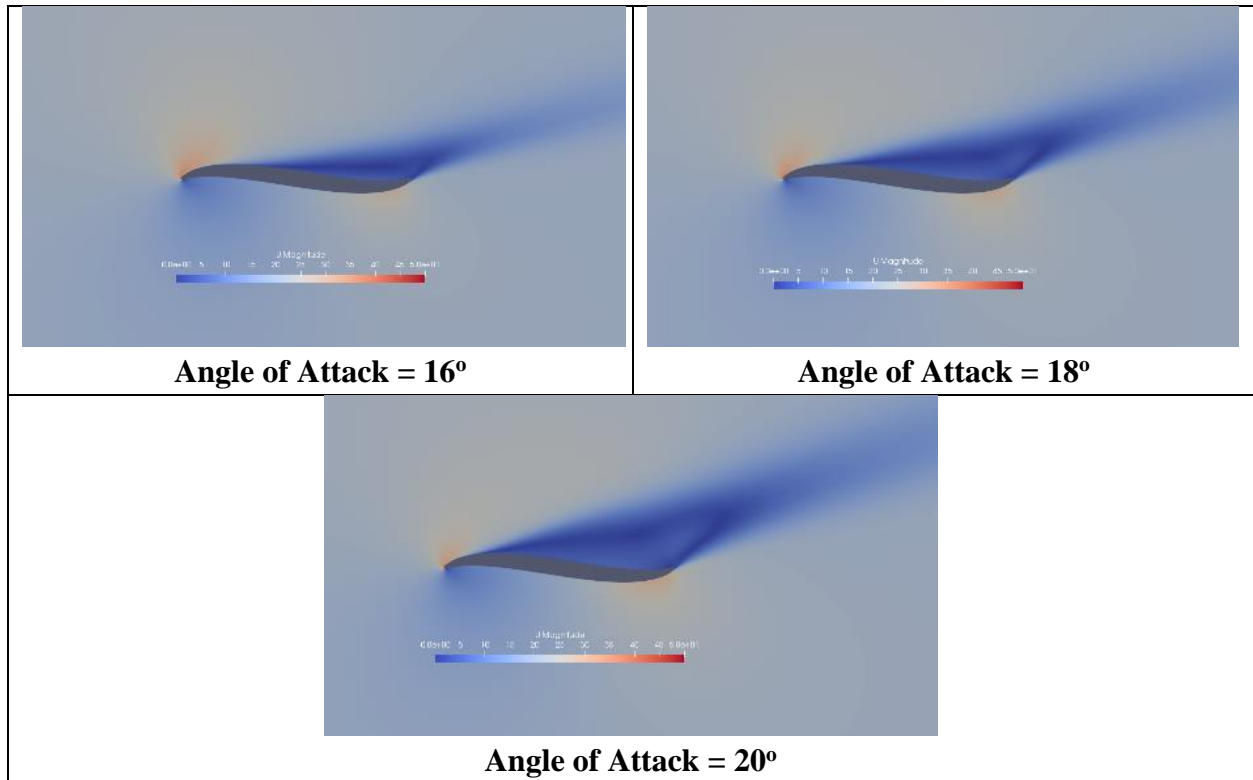
Figure 4.11 The Water Flow Pattern in various angles of attack for S–Shaped Airfoils

The pictures show that the water flows separately through the sharp leading edge of the S-Shaped airfoils to the upper and lower surface to the sharp trailing edge. In the angle of attack 0° and 2°, the velocity of water is lower on the upper surface and higher on the lower surface. Then, when the angle of attack increases between 4° and 12°, the velocity on the top surface near the leading edge is higher than at the bottom. It causes the airfoils to have the ability to lift and it is explained in **Fig. 4.7.** when the lift coefficient inclines. However, when the angle continues to rise above 14° to 20°, the water separation near the trailing edge starts spreading. In **Fig. 4.7.**, it can be seen that the lift coefficient is too high and causes the airfoils to lose their ability to lift. Furthermore, in **Fig. 4.9.**, the maximum lift-to-drag ratio for the S–Shaped airfoils is located on the angle of attack of 10°, so the airfoils' angle should be maintained slightly below the angle of attack of 10° to provide the optimum lift and aerodynamic efficiency.

4.2.6. Pressure

The pressure patterns in the various angles of attack can analyze the airfoils' ability to lift in different angles of attack. It can be shown in **Fig. 4.12.**

Angle of Attack = 0º

Angle of Attack = 2º
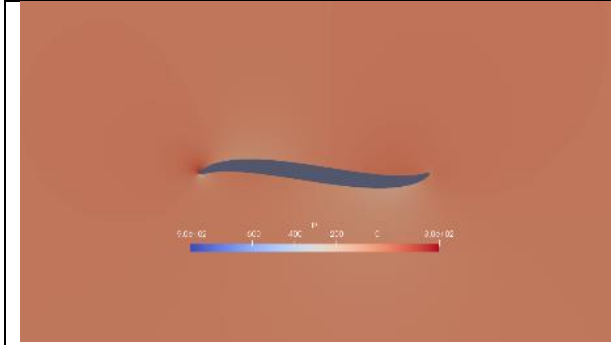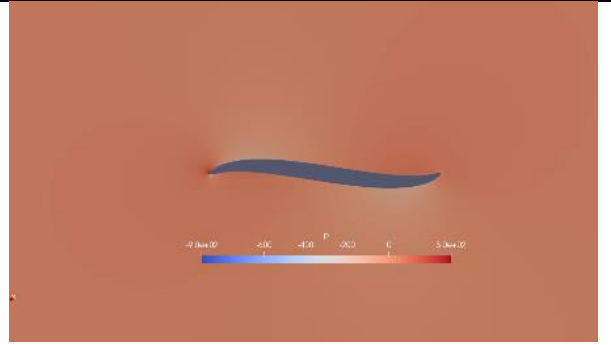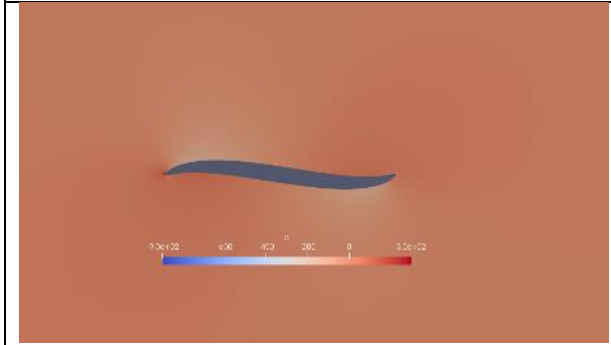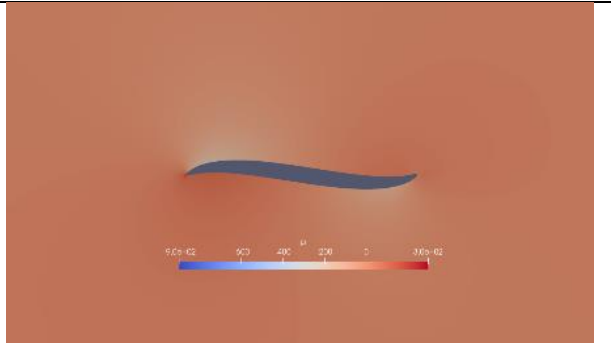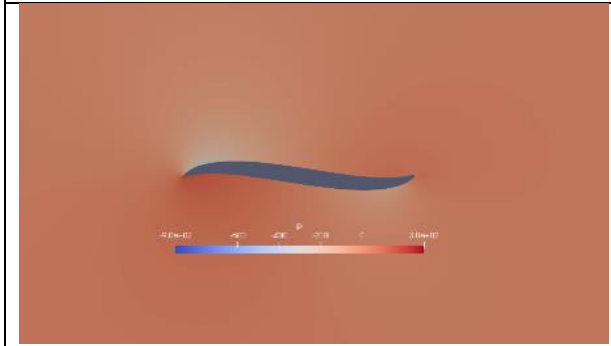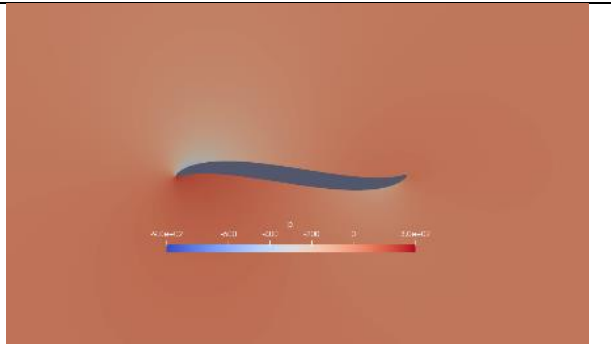

Angle of Attack = 4º

Angle of Attack = 6º

Angle of Attack = 8º

Angle of Attack = 10º

Angle of Attack = 12º

Angle of Attack = 14º
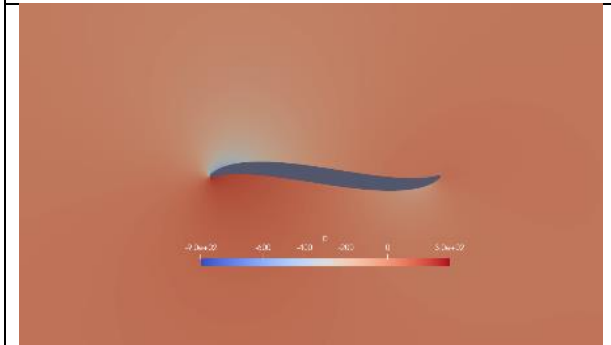
Angle of Attack = 16°	**Angle of Attack = 18°**
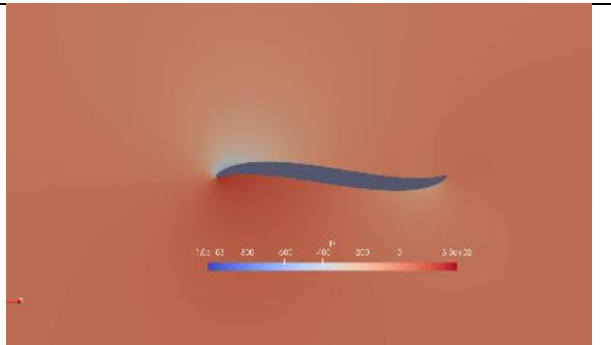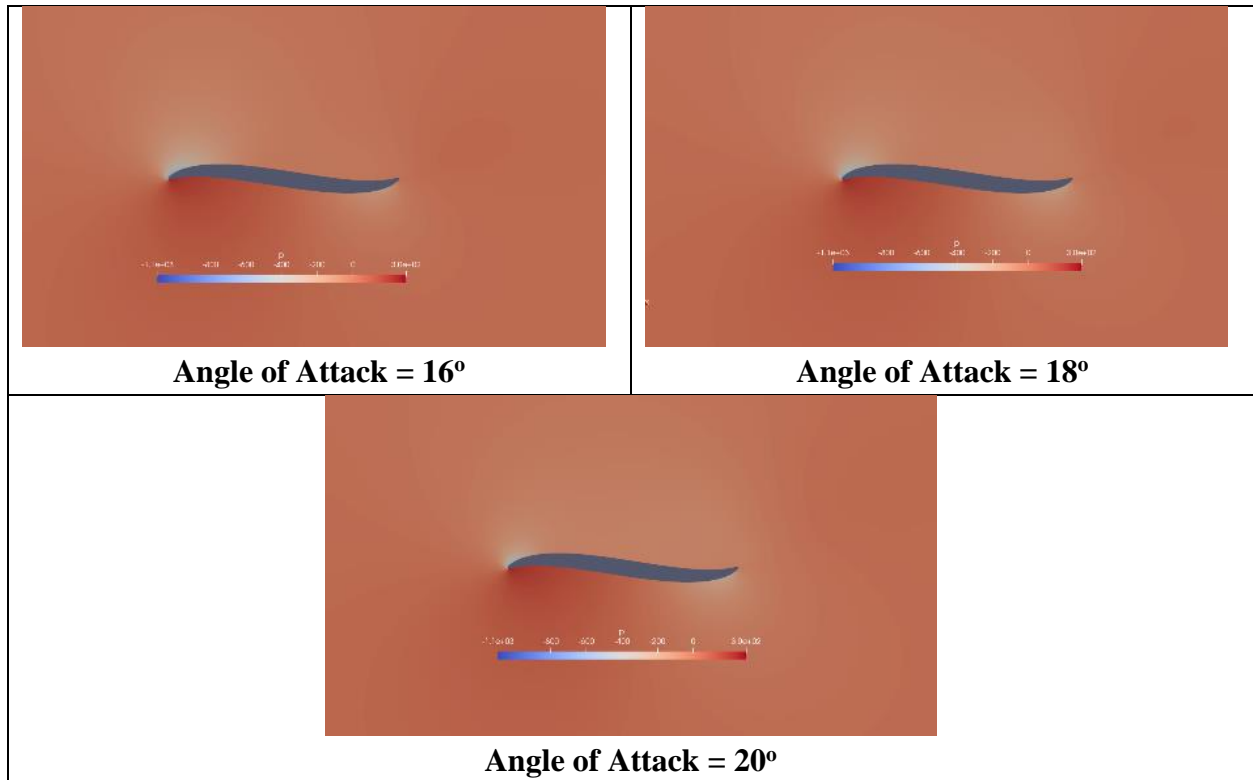
Angle of Attack = 20°

Figure 4.12 The Pressure in Various Angles of Attack for S - Shaped Airfoils

The pictures show that the pressure is higher on the upper surface near the sharp leading edge of the S-Shaped airfoils in the angle of attack of 0° and 2°. Then, when the angle increases between 4° and 12°, the pressure on the top surface near the leading edge is lower than at the bottom. It drives the airfoils to lift. However, in the angle of attack above 14° to 20°, when the pressure at the bottom of the airfoils is too high, the airfoils start to lose their performance.

4.3.   NACA – 0012 and S–Shaped Airfoils Comparison Result

The simulation results for all airfoils illustrate that the difference in angle of attack ($\Delta\alpha$) and the slope plays an important role in considering the airfoil performance and off–design performance.

To decide on the airfoils design for the horizontal axis tidal turbine, the simulation results for both NACA – 0012 and S–Shaped airfoils will be compared to the previous works. The current simulation results are compared in **Fig. 4.13.**, **Fig. 4.14.**, and **Fig. 4.15.**

Figure 4.13 The Plot of Lift Coefficient for NACA – 0012 and S–Shaped Airfoils

Figure 4.14 The Plot of Drag Coefficient for NACA – 0012 and S –Shaped irfoils
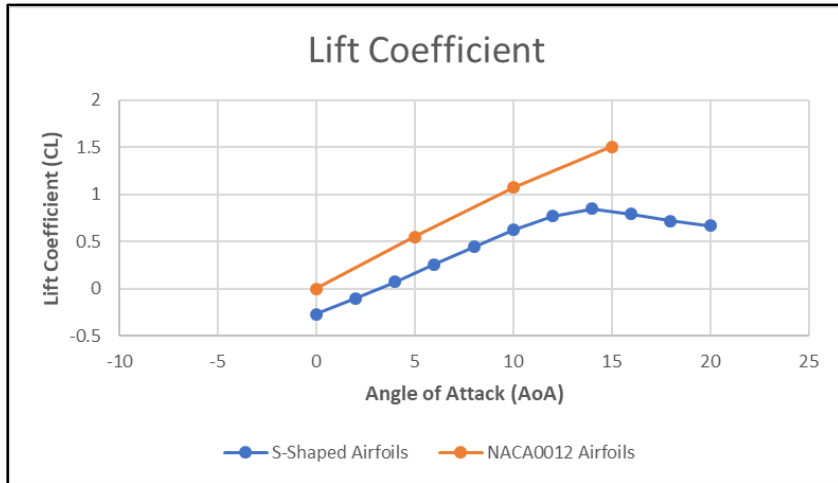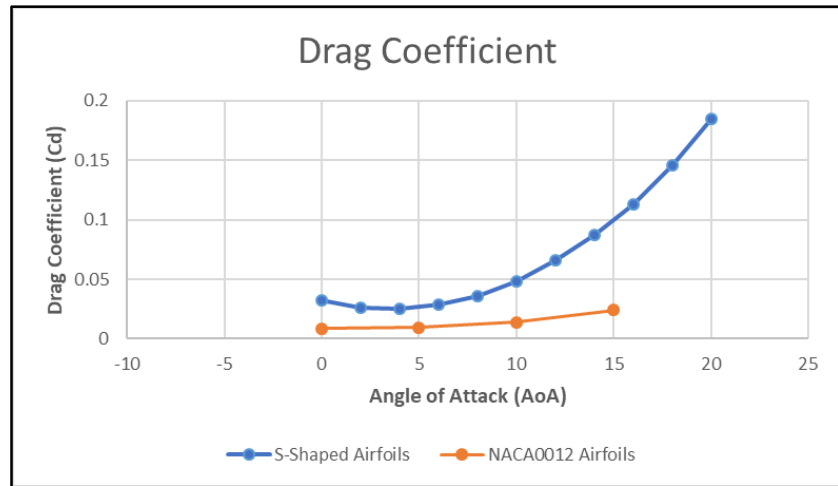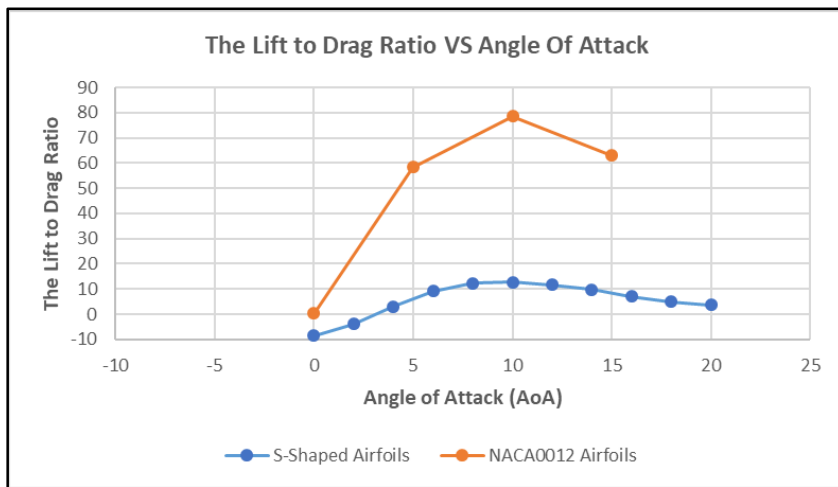

Figure 4.15 The Plot of Lift to Drag Ratio for NACA – 0012 and S–Shaped Airfoils

The current simulation result shows that NACA – 0012 airfoils have higher lift coefficient and lower drag coefficient than S–Shaped airfoils. Furthermore, the aerodynamic lift-to-drag ratio for NACA – 0012 airfoils have significantly higher than S–Shaped airfoils.

The airfoil performance and the drop–off design performance are summarized in **Table 4.3.** The maximum lift coefficient for NACA – 0012 airfoils is 1.6347 in the angles of attack of 17º which is higher than the maximum lift coefficient for S–Shaped airfoils which show 0.8458 in angle of attack of 14º. Then, the aerodynamic efficiency design for NACA – 0012 airfoils is 99.2199 in the angle of attack 12.13º which is also higher than the aerodynamic design for S–Shaped airfoils which is 12.7788 in 10º. It indicates NACA – 0012 airfoils have better performance than S–Shaped airfoils.

The difference in angle of attack ($\Delta\alpha$) between the maximum lift coefficient and the aerodynamic efficiency design for NACA – 0012 airfoils are larger than S–Shaped airfoil. It indicates the design for NACA – 0012 airfoils is further to the *stall* point than the S–Shaped. However, the slope for NACA – 0012 airfoils is also higher than S–Shaped airfoils which expected to be as lower as possible.

Table 4.3 The Aerodynamic Performance Parameter for NACA – 0012 and S–Shaped Airfoils

Airfoils	Lift Coefficient Max	Aerodynamic Efficiency Max	Aerodynamic Efficiency Design	Lift Coefficient design	Angle of Attack		$\Delta\alpha$	Slope
					Maximum	Design		
NACA0012	1.6347	64.89479952	99.2199688	1.272	17.24	12.13	5.11	6.717254
S-Shaped	0.8458484	9.705384206	12.7788391	0.6209574	14	10	4	0.768364

The previous work cases are taken from the computational investigation of the aerodynamic performance of reversible airfoils for a bidirectional tidal turbine (*Giljarhus, 2021*). It shows in **Table 4.4.** to compare results of different types of airfoils.

Table 4. 4 The Aerodynamic Performance Parameters for Different Airfoils

Airfoils	Aerodynamic Efficiency Max	Lift Coefficient design	Lift Coefficient Max	$\Delta\alpha$	Slope
NACA65-415	59.2	0.98	1.5	10	3.5
SYM65-015	38.9	0.76	0.9	8	1.83
ASYM54-415	46.3	0.67	0.86	4	3.25
B-Spline	54.5	1.11	1.3	4	1.01

Table 4.4. shows NACA65 – 415 airfoil has the highest maximum aerodynamic efficiency and maximum lift coefficient among the other airfoils. It indicates that NACA65 – 415 airfoil has the

highest performance. In addition, the B – Spline airfoil gives the closest result to NACA65 – 415 airfoils in terms of the maximum aerodynamic efficiency and maximum lift coefficient.

NACA65 – 415 airfoil also results in the highest difference angles of attack ($\Delta\alpha$), which means the design is the furthest to the *stall* point. Meanwhile, B – Spline shows the lowest design point which makes the design very close to the *stall* point. Therefore, the slope for NACA65 – 415 airfoils is the highest while the slope for B – spline is the lowest. The slope is expected to be as lower as possible.

The aerodynamic performance parameters from the previous work conclude NACA65 – 415 airfoil has the highest performance and the design is the furthest to *stall* point. Meanwhile, B – Spline airfoil is the second-highest performance despite the design is slightly closer to the *stall* point.

Based on the above discussion for all airfoils, S–Shaped airfoil has the worst performance and the closest to the *stall* point among the other airfoils.

Chapter 5: Conclusion

This thesis analyzed the airfoil shape design and the aerodynamic performance of the horizontal axis tidal turbine. Both NACA – 0012 airfoil and S–Shaped airfoil were simulated by the computational fluid dynamics (CFD) software, OpenFoam. The simulation provided some results that consist of the lift coefficient, the drag coefficient, the aerodynamic efficiency, the performance curve and the off–design performance, the water flow pattern, and the pressure.

NACA – 0012 was used to validate the computational setup. The simulation gave identical results to the experimental data. For lift-to-drag ratio, the simulation result was identical to the experiment data in lower angle of attack. However, in the angle of attack above 15º, the results showed a slightly lower lift-to-drag ratio. The performance curve showed NACA – 0012 airfoils have better performance than S–Shaped airfoils. Then, the off–design for NACA – 0012 airfoils was further to the *stall* point. Therefore, the slope for this airfoils was relatively higher than S-Shaped airfoils.

To decide the airfoils design for the horizontal axis tidal turbine, the S-Shaped airfoil results were compared to the previous works. It showed NACA65 – 415 airfoil design was the furthest to the *stall* point and have the highest performance. Meanwhile, S–Shaped airfoil was the worst performance and the closest to the *stall* point among the other airfoils.

This study only looked at a single S–Shaped airfoil, therefore, there could be performance improvement by looking at the other S–Shaped airfoil in the further study.

Bibliography

Buigues, G., Zamora, I., Mazon, A.J., Valverde, V., & Perez, F.J. (2006). Sea energy conversion: problems and possibilities. *University of Basque Country*.

Causes of climate change. European Commission. https://ec.europa.eu/clima/climate-change/causes-climate-change_en

Dincer, I. (2000). Renewable energy and sustainable development: a crucial review. *Renewable and Sustainable Energy Reviews, 4,* 157 – 175.

Douvi, E.C., & Margaris, D.P. (2012). Aerodynamic performance investigation under the influence of heavy rain of a NACA 0012 airfoil for wind turbine applications. *International Review of Mechanical Engineering (I.RE.M.E), 6.* Doi: 10.15866/ireme.v6i6.20761.

Giljarhus, K.E.T., Shariatpanahi, G.S., & Frøynes, O.A. (2021). Computational investigation of the aerodynamic performance of reversible airfoils for a bidirectional tidal turbine. *IOP Publishing Ltd.* doi: 10.1088/1757-899X/1201/1/012003.

Grabbe, M., Lalander, E., Lundin, S., & Leijon, M. (2009). A review of the tidal current energy resource in Norway. *Renewable and Sustainable Energy Reviews, 13,* 1898-1909. Doi: 10.1016/j.rser.2009.01.026.

Grasso, F. (2012). Design and optimization of tidal turbine airfoil. *Journal of Aircraft, 49,* 636-643. DOI: 10.2514/1.C031617.

Goundar, J.N., & Ahmed, M.R. (2013). Design of a horizontal axis tidal current turbine. *Applied Energy, 111,* 161-174. dx.doi.org/10.1016/j.apenergy.2013.04.064.

Imran, R.M., Hussain, D.M.A., & Soltani, M. (2016). An experimental analysis of the effect of icing on wind turbine rotor blades. *IEEE.* DOI: 10.1109/TDC.2016.7520041.

Li, W., Zhou, H., Liu, H., Lin, Y., Xu, Q. (2016). Review on the blade design technologies of tidal current turbine. *Renewable and Sustainable Energy Reviews, 63,* 414-422. dx.doi.org/10.1016/j.rser.2016.05.017.

Nicholls-Lee, R.F., & Turnock, S.R. (2008). Tidal energy extraction: renewable, sustainable and predictable. *Science Progress, 91(1),* 81-111. Doi: 10.3184/003685008X285582.

Orhan, K., Mayerle, R., & Pandoe, W.W. (2015). Assessment of energy production potential from tidal stream currents in Indonesia. *Energy Procedia, 76,* 7-16. Doi: 10.1016/j.egypro.2015.07.834.

Premkumar, T.M., Kumar, P., & Chatterjee, D. (2014). Cavitation characteristics of S-blade used in fully reversible pump-turbine. *Journal of Fluids Engineering, 136*, 1-15. DOI: 10.1115/1.4026441.

Premkumar, T.M., & Chatterjee, D. (2015). Computational analysis of flow over a cascade of s-shaped hydrofoil of fully reversible pump-turbine used in extracting tidal energy. *Renewable Energy, 77,* 240-249.

Renewable energy. Center for Climate and Energy Solutions. https://www.c2es.org/content/renewable-energy/#:~:text=Globally%2C%20renewables%20made%20up%2029,was%20added%20globally%20during%202020.

Renewables 2021. Global status report. REN21. https://www.ren21.net/wp-content/uploads/2019/05/GSR2021_Full_Report.pdf

Schubel, P.J., & Crossley, R.J. (2012). Wind turbine blade design. *Energies 2012, 5,* 3425-3449. DOI: 10.3390/en5093425.

Sheth, S., & Shahidehpour, M. (2005). Tidal energy in electric power systems. *IEEE.*

Shetty, C., & Priyam, A. (2022). A review on tidal energy technologies. *Materials Today: Proceedings, 56,* 2774-2779.

Suvanjumrat, C. (2017). Comparison of turbulence models for flow past NACA0015 airfoil using openfoam. *Engineering Journal, 21,* 207-221. DOI: 10.4186/ej.2017.21.3.207

U.S. Department of Energy. (2021, September 24). *Country analysis executive summary: Indonesia.* U.S. Energy Information Administration. https://www.eia.gov/international/analysis/country/IDN

U.S. Department of Energy. (2021, September 23). *Hydropower explained: Tidal power.* U.S. Energy Information Administration. https://www.eia.gov/energyexplained/hydropower/tidal-power.php

Wind turbine blade aerodynamics. *WE Handbook: Aerodynamics and Load, 2,* 1-10.

Zhu, F., Ding, L., Huang, B., Bao, M., & Liu, J. (2020). Blade design and optimization of a horizontal axis tidal turbine. *Ocean Engineering, 195,* 1-10. doi.org/10.1016/j.oceaneng.2019.106652.

(2018, February 26). *Construct2D (Computational fluid dynamics structured grid creator for 2D airfoils).* Sourceforge. https://sourceforge.net/projects/construct2d/

(2021, May 11). *Electricity production.* Energi Fakta Norge. https://energifaktanorge.no/en/norsk-energiforsyning/kraftproduksjon/

(2021, July 22). *Fossil fuels.* Environmental and Energy Study Institute. https://www.eesi.org/topics/fossil-fuels/description#:~:text=Overview,percent%20of%20the%20world's%20energy

(2022, April). *Total renewable power generation capacity in Indonesia from 2012 to 2021.* Statista Research Department. https://www.statista.com/statistics/872498/total-renewable-power-generation-capacity-in-indonesia/#statisticContainer